

Article

Highly Efficient Hybrid Reconfigurable Intelligent Surface Approach for Power Loss Reduction and Coverage Area Enhancement in 6G Networks

Aya Kh. Ahmed  and Hamed S. Al-Raweshidy * 

Department of Electronic and Electrical Engineering, College of Engineering, Design, and Physical Science, Brunel University London, London UB8 3PH, UK; aya.ahmed@brunel.ac.uk

* Correspondence: hamed.al-raweshidy@brunel.ac.uk

Abstract: This paper introduces a novel efficient hybrid reconfigurable intelligent surface (RIS) approach designed to significantly reduce power loss and enhance coverage area in 6G networks. The core innovation of this approach lies in an advanced iterative algorithm introduced as the Hybrid reconfigurable intelligent surface decision-making algorithm (HRIS-DMA) that integrates precise user location data into the RIS configuration process. By dynamically adjusting RIS elements to reflect and direct signals based on real-time user positions, this method minimises signal attenuation and optimises signal propagation. The mechanism driving the performance gains includes precise beamforming and intelligent reflection, continuously refined through iterative updates. This technique ensures robust signal strength and expanded coverage, addressing the challenges of dense and diverse deployment scenarios in 6G networks. The proposed scheme's application in 6G networks demonstrates substantial improvements in signal quality and network reliability, paving the way for enhanced user experiences and efficient communication infrastructures. This novel approach was tested using MATLAB R2023a, and its performance was evaluated using three downlink scenarios: zero to few, few to moderate, and moderate to many obstacles. The three scenarios show higher coverages than conventional simultaneous transmitting and reflecting reconfigurable intelligent surfaces (STAR-RISs) and base station (BS) handover. Based on the evaluation metrics, the analysis results of the novel HRIS-DMA show 70% less signal power loss, 0.17 μ s less system delay, 25 dB and 12 dB channel gain compared with the conventional STAR-RIS and BS handover, respectively, and 95% improvement in the overall system's efficiency compared to STAR-RIS and 13% compared to BS-BS handover.

Keywords: coverage; power optimisation; reconfigurable intelligent surface; simultaneous transmission and reflection; terahertz; 6G



Citation: Ahmed, A.K.; Al-Raweshidy, H.S. Highly Efficient Hybrid Reconfigurable Intelligent Surface Approach for Power Loss Reduction and Coverage Area Enhancement in 6G Networks. *Appl. Sci.* **2024**, *14*, 6457. <https://doi.org/10.3390/app14156457>

Academic Editor: Christos Bouras

Received: 1 July 2024

Revised: 17 July 2024

Accepted: 23 July 2024

Published: 24 July 2024



Copyright: © 2024 by the authors. Licensee MDPI, Basel, Switzerland. This article is an open access article distributed under the terms and conditions of the Creative Commons Attribution (CC BY) license (<https://creativecommons.org/licenses/by/4.0/>).

1. Introduction

Today, 6G networks have the potential to completely transform the Internet of Things (IoT) by facilitating applications that require ultra-low latency, broader spectrum resources, improved energy efficiency (EE), and widespread network coverage. These prerequisites are essential for the smooth operation of many Internet of Things scenarios, such as industrial automation, self-driving cars, smart cities, and remote healthcare [1,2]. To accomplish these objectives, enhancements to the current communication technologies [3], which have already demonstrated their efficacy, have been suggested. These enhancements include ultra-massive multiple-input multiple-output capacity (UM-MIMO), ultra-dense networks (UDNs), and terahertz (THz) communication. Nevertheless, the continuous growth in the number of antennas/base stations (BSs) and the utilisation of extremely high carrier frequencies may result in higher energy consumption and hardware expenses. This is due to the necessity of installing more power-intensive and expensive radio frequency (RF) chains for signal conversion. However, deploying many active components that operate

simultaneously at extremely high frequencies in wireless networks may only sometimes be advantageous, as doing so can introduce new challenges, including complex interference scenarios between users and cells, pilot contamination, and significant hardware impairments.

Developing novel and economical methodologies for wireless communication systems is imperative to address the above-mentioned constraints. Driven by the rapid progress in metasurfaces and advanced fabrication technologies, reconfigurable intelligent surfaces (RISs) have emerged as highly promising solutions [4–7]. A RIS is a two-dimensional human-made surface containing many low-cost passive elements. In utilising a smart controller connected to the RIS, the main advantage of the RIS is the ability to modify the direction of the wireless signals received by the RIS by manipulating the specific phase response of each element [5,8]. Unlike conventional multi-antenna and relaying concepts that involve the active generation of wireless signals using expensive RF chains, RISs recycle existing signals in a network passively without requiring RF chains. Therefore, RISs are more cost-effective and ecologically sustainable than traditional active antenna systems. In addition, RISs can be easily incorporated into current wireless networks by installing them on various structures, including roadside billboards, building tops, building facades, windows, and even clothing worn by individuals [6,9].

There are diverse approaches to integrating RISs in communication systems, which generally can be classified into different approaches, include reducing power consumption during transmission [10–14], improving spectra and EE [4,15–26], and creating an unobstructed LoS [27–34]; a full analysis for the work addressed in previous researches is described in Section 3.

Although the current STAR-RIS approaches elaborate on the improvement of communication systems, it still have some restrictions on the freedom of the communication systems. Currently, the transmitter and receiver must be positioned on the same side of the RIS, resulting in a radio coverage environment that covers only half of the surrounding space, either the reflection area or transmission area, as in Figure 1a,b. Nevertheless, the practical implementation of geographical limitations might only sometimes be adhered to, particularly when considering the more demanding requirements of the upcoming wireless generation of 6G. This limitation significantly restricts the adaptability and efficiency of RISs, as users are typically situated on both sides of an RIS.

The innovative idea of transmitting and reflecting an RIS (T/R RIS) simultaneously was introduced to address this constraint in [35–37]. In particular, as shown in Figure 1c, the wireless signal that reaches an element of a T/R RIS from either side of the surface is split into two separate components [38]. The incident signal is divided into two parts: the reflected signal, which is directed back to the same area as the incident signal, and the transmitted signal, which is sent to the opposite area from the incident signal. As this approach sounds promising, however, the T/R RIS in its current state splits the signal power between the reflected signal and transmitted signal for the same user [35–37], which means that if the user is located in the transmission area, half of the signal power allocated for that user will be reflected. This will cause problems of high interference in the reflection area and signal weakness in the transmission area.

In order to solve the aforementioned problems [35,37], manipulating the electric and magnetic currents of a T/R RIS element allows for the reconfiguration of transmitted and reflected signals. This can be achieved through two distinct coefficients, namely, the transmission coefficient and the reflection coefficient, which are normally independent of each other. Thus, achieving a highly adaptable radio environment that covers the entire space is possible. However, the interference problem in the reflection area is controlled by signal distractions, but this approach does not solve the signal weakness in the transmission area.

In order to solve this, Ref. [38] presents three operational procedures for T/R RISs: energy splitting (ES), mode switching (MS), and time switching (TS). Their results demonstrate superior EE for the BS; however, this was not observed for the T/R RISs, a particularly relevant consideration for the user. The suggested modes simply synchronise the transmis-

sion producer and do not simultaneously execute transmission and reflection.

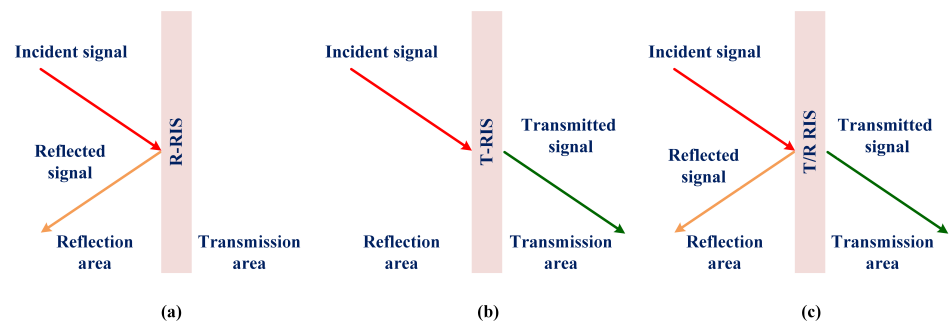


Figure 1. The concept of simultaneously transmitting and reflecting RISs. (a) Reflecting only. (b) Transmitting only. (c) Transmitting and reflecting.

In [39], each component of the described T/R RIS prototype consists of a parallel resonant tank and small metallic loops that supply the necessary electric and magnetic surface reactance. Despite the aforementioned benefits, the exploration of integrating T/R RISs into wireless communication systems is still in its early stages.

The authors of [40] proposed an intelligent omni-surface (IOS) to attain complete coverage in all directions, similar to the concept of T/R RISs. However, contrary to T/R RISs, IOSs exhibit identical phase shifts for transmission and reflection due to the presence of positive-intrinsic-negative (PIN) diodes in the IOS elements, which control the phase shifts.

In [41], the authors introduced hybrid RISs by enabling the passive element to reflect the impinging signal in a controllable manner while simultaneously sensing another rounded signal. This sensing ability makes it possible to facilitate various functions related to network management, including the estimation of channels and localisation. Even though this implementation introduces a new idea for a RIS, it increases interference and power loss for signal reflection in the system without making signal transmission more effective.

Just recently, [42] introduced a hybrid active–passive RIS into a wireless system. However, the proposed solution managed to deliver a lower outage probability but failed to adhere to the signal power loss problem, limited coverage area, and high-density levels.

The higher 6G demands, the lack of imperative solutions using efficient operational methods for T/R RISs in the 6G era, and the limitations of the associated optimisation techniques for joint transmission and reflection beamforming in T/R RIS-assisted wireless networks are the motivations of hybrid RISs in this study.

The rest of this paper is organised as follows. Section 2 lists this paper’s contributions. The most recent related works are highlighted in Section 3. In Section 4, the system model methodology is described. In Section 5, the HRIS-DMA novel algorithm is presented. The implementation scenarios for model analysis are presented in Section 6. Section 7 is dedicated to discussing the performance analysis. The concluding remarks and outlines for future developments are presented in Section 8.

2. Paper Contributions

In order to exploit the full potential of RISs in 6G, in this paper, we introduce a novel power optimisation algorithm. The proposed iterative algorithm operates by continuously updating the configuration of the RIS elements based on real-time user location data. By precisely aligning the RIS elements to reflect and direct the incoming signals toward the exact positions of the users, the algorithm minimises signal attenuation and maximises signal strength at the user end. This targeted approach not only reduces power loss but also significantly enhances the coverage area by ensuring that the signal is optimally directed, even in challenging environments with high user density and obstacles. Performance gains are achieved through a combination of precise beamforming and intelligent reflection, which are continuously refined through iterative updates. The algorithm enables full transmission and reflection capacity in a hybrid form called a hybrid reconfigurable intelligent

surface (HRIS). Additionally, this paper explores the design of a hybrid transmission and reflection beamforming approach for multicast communication in three distinct scenarios.

The main contributions of this paper can be summarised as follows:

- We introduce an HRIS into a wireless communication system to assist transmission. In this system model, we identify a decision-making algorithm, HRIS-DMA, that optimally transforms signal power into either full transmission mode or full reflection mode without any power loss in the incident signal.
- We incorporated the user's location in the HRIS-DMA to provide a direct line of sight (LoS) for blocked users located in the transmission area without signal power loss. We verify the advantages of HRIS-DMA via MATLAB simulation and further analysed the simulation results.
- Three different downlink transmission scenarios are presented to characterise the terahertz frequency band (300–500 GHz) and different levels of user density with a maximum density of 16×10^6 , which are anticipated to be standardised in the 6G era.

3. Related Works

In light of the beneficial characteristics of RISs mentioned previously, many researchers have explored the potential benefits of RIS-aided systems in wireless networks. These benefits include reducing power consumption during transmission [10–14], improving spectra and EE [4,15–26], and creating an unobstructed LoS [27–34].

More specifically, the authors of [10] proposed an alternating optimisation approach for pieces of user equipment (UE) sensing based on their size and identified a trade-off in joint beamforming between sensing the target user size and the real communication operation. Under specific constraints, the authors in [11] jointly optimised the active beamforming vector at the access point (AP) and reflection beamforming at the RISs to maximise the received Signal-to-Noise Ratio (SNR) of a single user and the sum rate of multiple users, respectively. The authors of [12] employed joint beamforming to increase energy collecting and information transfer with uplink and downlink for Internet of Things (IoT) devices.

Moreover, in [13], the authors proposed a hybrid networking structure that utilises cascaded and parallel RIS beamforming topology. The cascade alignment reduces path loss and improves multiplicative gain, while the parallel alignment boosts scattering signatures within the desired cluster. On the other hand, the authors of [14] employed the block denationalisation method to express the beamforming matrices of the BS and the users through the phase shifts of a RIS. Subsequently, they proposed a manifold method for enhancing beamforming optimisation by replacing the beamforming matrices of the BS and the users with their respective expressions.

In order to improve EE and the coverage area, the authors of [15,18,20] used an unmanned aerial vehicle (UAV) with an RIS for downlink and uplink communication to assist the connection between the BS and UE; although this sounds very promising, the complexity and interference that the pieces of UE face are neglected.

Furthermore, a RIS-aided multiple-input multiple-output (MIMO) system's communication spectrum optimisation and energy were characterised in [16,17,19,24,25], where the authors used active RF chains to optimise transmission power and reduce system delay. Additionally, the mmWave multiple-input single-output (MISO) system EE optimisation problem was addressed in [21,22]. A swarm optimisation algorithm was used in [21] for RIS phase shifting to maximise the EE in the sine-cosine approach, while the authors of [22] used visible light communication technology to achieve the same objectives. The authors of [23,26] optimised the EE and the bit error rate of a RIS-aided communication system by utilising the channel state information via compressive sensing techniques and a uniform planner array, respectively. The authors of [27,30] provided a pathway of reflection that involved multiple hops over both active and passive RISs. Specifically, the active RISs have the ability to strategically amplify the reflected signal over the multi-reflection connection, thereby counteracting the significant loss of signal strength due to distance and optimising

energy efficiency. In [28,29,31–34], a multi-RIS approach is introduced in which all the used RISs are passive. The used approaches were designed to maximise the sum rate in mmWave systems and provide a direct LoS.

In addition, Table 1 shows a comparison of the current state-of-the-art methods for the conventional T/R RIS and their achievement in providing wireless communication systems that have addressed and solved the need for higher reliability, lower delay, higher area coverage, less power loss, and higher system efficiency compared to the novel HRIS-DMA.

Notation: All the parameters that are not defined inside the text are identified in Table 2, which presents the mutual design parameters.

Table 1. Comparison table of related work.

Reference	Year	Reliability	Delay	Coverage	Power Loss	Efficiency
[10]	2023	✗	✗	✗	✓	✗
[11]	2023	✗	✗	✗	✓	✗
[12]	2023	✗	✗	✗	✓	✗
[13]	2023	✗	✗	✗	✓	✗
[14]	2023	✗	✗	✗	✓	✗
[15]	2023	✗	✓	✓	✗	✗
[16]	2023	✗	✓	✗	✓	✗
[17]	2023	✗	✓	✗	✓	✗
[18]	2023	✗	✓	✓	✗	✗
[19]	2023	✗	✓	✗	✓	✗
[20]	2023	✗	✓	✓	✗	✗
[21]	2023	✗	✗	✗	✗	✓
[22]	2023	✗	✗	✗	✗	✓
[23]	2023	✓	✓	✗	✓	✓
[24]	2023	✗	✓	✗	✓	✗
[25]	2023	✗	✓	✗	✓	✗
[26]	2023	✓	✓	✗	✓	✓
[27]	2023	✗	✗	✗	✓	✗
[28]	2024	✓	✗	✗	✗	✗
[29]	2023	✓	✗	✗	✓	✗
[30]	2023	✗	✗	✗	✗	✗
[31]	2023	✓	✗	✗	✗	✗
[32]	2023	✓	✗	✗	✗	✗
[33]	2023	✓	✗	✗	✗	✗
[34]	2021	✓	✗	✗	✗	✗
[35]	2021	✗	✗	✓	✗	✗
[36]	2022	✗	✗	✓	✗	✗
[37]	2022	✗	✗	✓	✗	✗
[40]	2023	✗	✗	✓	✗	✗
[43]	2023	✗	✗	✓	✗	✓
[42]	2024	✗	✓	✗	✗	✗
[44]	2024	✗	✓	✓	✗	✗
[45]	2024	✗	✗	✗	✗	✓

Table 1. Cont.

Reference	Year	Reliability	Delay	Coverage	Power Loss	Efficiency
[46]	2024	✗	✗	✓	✓	✗
[47]	2024	✓	✗	✗	✗	✗
[48]	2024	✓	✗	✗	✗	✗
[49]	2024	✓	✗	✗	✓	✗
[50]	2024	✓	✗	✗	✗	✗
[51]	2024	✓	✗	✗	✗	✗
[52]	2024	✓	✗	✗	✗	✗
[53]	2024	✗	✗	✗	✗	✓
[54]	2024	✗	✗	✓	✗	✗
[55]	2024	✗	✗	✗	✗	✓
This work	2024	✓	✓	✓	✓	✓

Table 2. Mutual model design parameters.

Parameter	Definition
$M = 15$	Number of HRIS elements
l_M	10 (cm)
N_θ	Number of phase shifts, where $N_\theta = \{0, \dots, 2n\pi/N_\theta, \dots, 2(N_\theta - 1)\pi/N_\theta\}, 1 \leq n \leq N_\theta - 1$
U_{AG}^n	User antenna gain
S	Power density
Z_{air}	Air impedance
E_r	Electric field
A_e	Effective aperture
A_{HRIS}	HRIS effective aperture
P_s	Signal power
l_{HRIS}^U	Distance between HRIS and user
l_{HRIS}^{BS}	Distance between HRIS and BS
NP^{BS}	BS normalised power radiation
NP^U	User normalised power radiation
$NP^{HRIS,BS}$	HRIS normalised power radiation from BS
$NP^{HRIS,U}$	HRIS normalised power radiation directed toward user
$A_{r,t}$	Signal amplitude response
CSI_{inst}	Instantaneous channel state information
CSI_{stat}	Statistical channel state information
$I_{response}$	Impulse response
DF	Digital filter
FD	Fading distribution
CH_{gain}	Channel gain
R_M	Reflection/transmission coefficient, which equals $ R_M \exp(-j\phi_M) \exp(-j\frac{2\pi}{\lambda}(l_{HRIS}^{BS} + l_{HRIS}^U))$

4. System Modelling Methodology

In this section, a novel design and implementation for HRIS-DMA is studied, which will enable the HRIS to transmit and reflect the incident signal effectively with lower signal power loss. The mutual system requirements, channel model, power optimisation model, and decision-making algorithm are demonstrated by conducting tests and comparing three distinct transmission situations utilising varying sets of THz frequencies. The system design architecture considers the city's layout, which includes tall buildings, high trees, narrow alleys, and blocked users. The network profile depicted in Figure 2 is a model area architecture that closely resembles the implemented design.

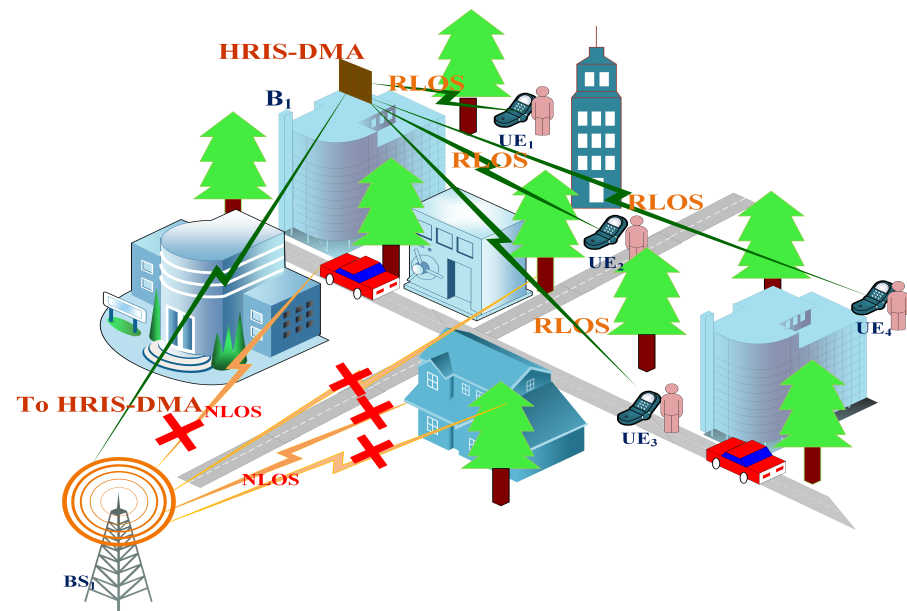


Figure 2. Illustration of an HRIS-DMA-aided downlink communication system, where obstacles block the direct BS–user links. LOS → line of sight, RLOS → redirected line of sight, and NLOS → no line of sight.

In this model, the BS serves as the central node that transmits data to the users. It must have high transmission power and be capable of handling multiple user connections simultaneously. The BS sends the downlink signals to the HRIS, which then redirects the signals toward the UE. The HRIS is deployed to enhance signal propagation and coverage by intelligently reflecting the signals received from the BS. The HRIS is equipped with a dynamic DMA that can adjust its reflective properties based on real-time user location data. The HRIS modifies the phase and amplitude of the incoming signals to focus them toward the intended UEs, thereby improving signal strength and coverage. The control unit processes location and signal quality data from the UEs and instructs the HRIS on how to adjust its reflective elements to optimise the communication link using the novel DMA.

The choice of HRIS elements was made by considering both computing efficiency and comprehensive coverage of critical functions by balancing the system's complexity and performance. The number of elements in the field of HRIS can vary based on the individual requirements and complexity of the system. In comparable studies and real-world applications, 10–20 components are commonly employed to provide optimal performance without excessive intricacy. Research articles such as [56–58] and practices in the business frequently have utilised a comparable set of components to guarantee thorough functionality without unnecessarily complicating the model. The algorithm's design guarantees its suitability for real-world networks by prioritising certain features such as scalability, adaptability, and interaction with existing infrastructure. This enables implementation in practical situations, such as smart cities and improved wireless networks.

In this study, the system under consideration was single-user multiple-input multiple-

output (SU-MIMO) to meet the specific application scenario, performance advantages, and experimental setup. It is worth mentioning that the system is applicable to be expanded to a multi-user MIMO system with a much-complicated beamforming design to minimise inter-user interference.

4.1. HRIS-DMA Mutual Design Parameters

Figure 2 shows an illustration of the HRIS-DMA collaborative transmission system. In this network, we considered an HRIS-aided downlink communication system operating over a THz frequency, where the p^{th} antenna of BS₁ communicates with multiple single-antenna users with the aid of an HRIS that consists of M elements. In this paper, we assume that obstacles block the direct links between the BS and the users in the presented network, as this is the most challenging scenario in conventional communication systems. To ensure simplicity of presentation and reveal fundamental design properties, the network shown in Figure 2 resembles a wireless communication network. In this network, we explain the concept of HRIS-DMA for only four blocked users UE _{n} , one BS, and one HRIS located on top of building number one B₁; all users are blocked from the BS by obstacles.

The network in Figure 2 shows that the HRIS is located on top of B₁, and it is designed with M patches, each of which has a 100 cm² patch size, with 0.01 mm of air space between them. Additionally, the mutual HRIS design parameters, which are fixed through the testing process, are the HRIS element response, $|\Gamma_m| = 0.9$; signal power, $P_s = 45$ dBm; wavelength, $\lambda = 0.001$ m; HRIS antenna gain, $G_{HRIS} = 1$; and power radiation parameters, $\epsilon_r = \epsilon_t = 0.99$.

As a start, we perform an initial test to check the signal redirection with full power as demonstrated in Figure 3. In this, we prove that the HRIS-DMA performs signal transmission with full signal power; additionally, the full signal beam is directed toward the user in the transmission area with different angles and different user locations. Moreover, to fully understand the maximum performance improvement offered by HRIS-DMA, it is anticipated that the BS will have access to the instantaneous and statistical channel state information CSI _{$ints,stat$} for all channels, as analysing them is beyond the scope of this study.

The next step is to optimise the HRIS-DMA, which was designed and controlled by an HRIS controller to transmit or reflect the incident signals simultaneously based on real-time user positions continuously refined through iterative updates.

As shown in Figure 3, the new signal redirection keeps the signal power focused toward the intended user in one direction. It does not split the signal into the transmission and reflection areas as in the conventional T/R RIS.

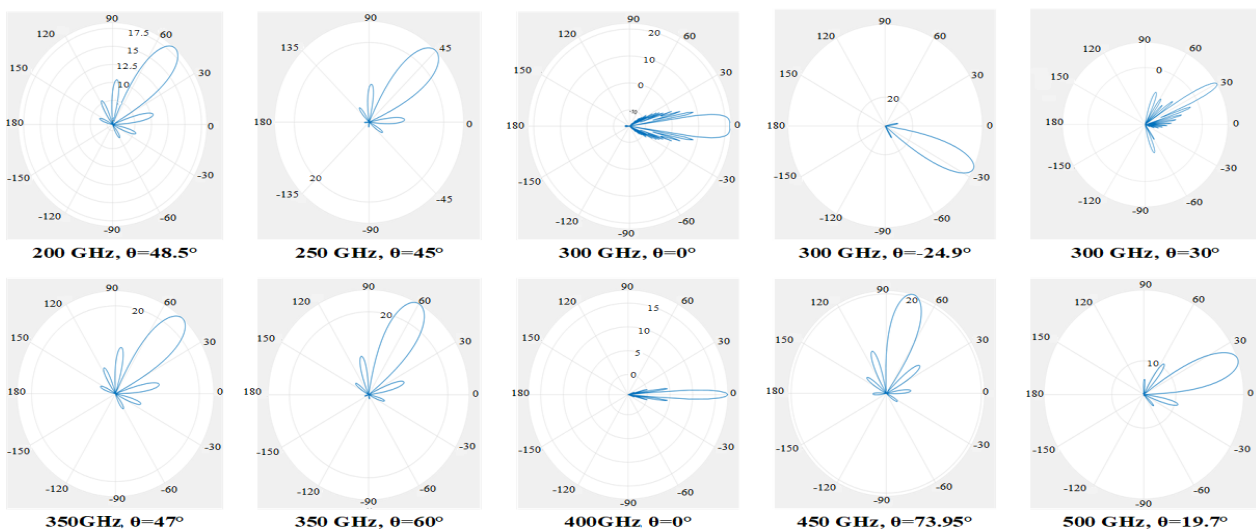


Figure 3. Redirecting user signal with focused beamforming.

4.2. Basic Signal Model

Figure 1c shows that the wireless signal incident on a given element of the conventional T/R RIS is divided into transmitted and reflected signals. To characterise this RIS feature, let S_m denote the signal incident on the m^{th} element of the T/R RIS, where $m \in M \triangleq 1, 2, \dots, M$. The signals transmitted and reflected by the m^{th} element can be modelled as $x_m^t = (\sqrt{\beta_m^t} e^{j\theta_m^t}) S_m$ and $x_m^r = (\sqrt{\beta_m^r} e^{j\theta_m^r}) S_m$ [37], where $\sqrt{\beta_m^t} \in [0, 1]$, $\theta_m^t \in [0, 2\pi)$, and $\sqrt{\beta_m^r} \in [0, 1]$, $\theta_m^r \in [0, 2\pi)$ are the amplitude and phase shift response of the m^{th} element's transmission and reflection coefficients, respectively. In practical scenarios, the phase shifts (i.e., θ_m^t and θ_m^r) can be chosen independently of each other. On the other hand, the adjustments for the amplitude coefficient (i.e., $\sqrt{\beta_m^t}$ and $\sqrt{\beta_m^r}$) are coupled. Thus, the sum of the transmitted and reflected signal powers must be equal to the power of the incident signal, which should satisfy each element's condition in (1).

$$\beta_m^t + \beta_m^r = 1, \quad \forall m \in \mathcal{M} \tag{1}$$

Accordingly, the conventional operating protocol for a T/R RIS splits the power of the incident signal between the transmitted and reflected signals, with a splitting ratio of $\beta_m^t : \beta_m^r$. In this case, the transmission and reflection coefficient matrices are given as in (2) and (3), respectively, in which $\beta_m^t, \beta_m^r \in [0, 1]$ and $\theta_m^t, \theta_m^r \in [0, 2\pi], \forall m \in \mathcal{M}$. As can be noticed, both coefficients can be optimised, resulting in a higher degree of flexibility in the communication system's design. However, the conventional protocol wastes half of the signal power, resulting in less coverage and higher power loss.

$$\Theta_t^{ES} = \text{diag} \left(\sqrt{\beta_1^t} e^{j\theta_1^t}, \sqrt{\beta_2^t} e^{j\theta_2^t}, \dots, \sqrt{\beta_M^t} e^{j\theta_M^t} \right) \tag{2}$$

$$\Theta_r^{ES} = \text{diag} \left(\sqrt{\beta_1^r} e^{j\theta_1^r}, \sqrt{\beta_2^r} e^{j\theta_2^r}, \dots, \sqrt{\beta_M^r} e^{j\theta_M^r} \right) \tag{3}$$

4.3. Channel Model

As mentioned in Section 4.1 and illustrated in Figure 1, the utilisation of the standard T/R RIS in its present state inevitably leads to a 50% loss in signal power, reducing the coverage area during transmission. This is in contrast to the novel HRIS-DMA technique discussed in this research. In order to provide a clear and concise explanation of the new HRIS, the channel model must be clarified first. This channel model adjustment is crucial for assessing the effectiveness of the communication network supported by the HRIS-DMA.

Let H be the channel matrix between the BS and the users and $[H]_{n,p} \triangleq h^{(n,p)}$ be the gain from the BS p^{th} antenna to the user n . Path loss, fast fading, and HRIS responses are considered when modelling the channel. Then, the single channel model between the m^{th} HRIS element, and the BS p^{th} antenna and user n is given by

$$\hat{h}_m^{(n,p)} = \sqrt{\alpha_m^{(n,p)}} g_m^{(n,p)} \Gamma_m^n \tag{4}$$

where $\alpha_m^{(n,p)}$ represents path loss, $g_m^{(n,p)}$ is the fading coefficient with zero mean and independent unit variance for different HRIS channels, and Γ_m^n represents the HRIS element response. The path loss, on the other hand, is modelled as in 5:

$$\alpha_m^{(n,p)} = \frac{\lambda^2 G I_M^2 G_{HRIS} F_m^p F_m^n}{M (D_m^p D_m^n) \gamma} \tag{5}$$

where λ is the wavelength, G represents BS antenna gain, γ is the path loss exponent, F_m^p is the radiation power at the m^{th} HRIS signal received from the p^{th} BS antenna, F_m^n is the signal power radiation from the m^{th} HRIS antenna to the user n , G_{HRIS} is the HRIS antenna gain, and D_m^p and D_m^n are the distance between the base station and HRIS element antenna and the distance between the HRIS element and users, respectively.

The effect of user location and angle with respect to the BS and HRIS was elucidated by modelling and measuring the signal power radiation as in (6) and (7), respectively. In (7), the determination of the ε value depends on the user's location in the transmission area or reflection area. Thus, (4) can be expressed as in (8), with an average path loss value.

$$F_m^p = \cos^2 \theta_m^p G_{HRIS} \quad (6)$$

$$F_m^n = \cos^2 \theta_m^n \varepsilon_{(t,r)} \quad (7)$$

$$h^{(n,p)} = \sum_{m=1}^M \hat{h}_m^{(n,p)} = \sqrt{\hat{\alpha}^n} \sum_{m=1}^M g_m^{(n,p)} \Gamma_m^n \quad (8)$$

5. HRIS-DMA Novel Algorithm

In this section, we describe the decision-making algorithm introduced into the HRIS controller to enable the hybrid ability of HRIS elements to transmit and reflect an incident signal simultaneously. This algorithm models the incident signal moving toward the intended user without wasting 50% of signal power. The details of the developed algorithm are summarised in Algorithm 1. User location d_{ue} from the BS is the main factor determining the allocated power of transmission or reflection in this work. Accordingly, this decision will be affected by the user's location according to the HRIS, defined as $D_{p(trans,ref)}$.

The working methodology starts with the parameter initialisation of the parameters for the BS, HRIS, and UE. Set initial conditions for the DMA within the HRIS. Then, the system design continuously monitors and updates the exact location of each UE within the coverage area. Use real-time data to feed the HRIS configuration process. After that, the signal is transmitted from the BS to the HRIS by adjusting the HRIS elements based on the iterative algorithm to optimise signal reflection toward the UEs.

As a real-time adjustment, the system will continuously update the HRIS configuration to adapt to changes in UE location and network conditions, and optimise the signal path to reduce power loss, minimise latency, and improve coverage. Additionally, the performance metrics, such as signal strength, coverage area, failed signal rate, and system efficiency, are measured and compared against predefined KPIs for 6G networks. As the algorithm is iterative, we implemented a feedback mechanism to continuously refine the HRIS adjustments based on real-time performance data, which ensures system adaptations to dynamic network conditions and user movements.

As the targeted validation property for network communication in this work is to provide a higher coverage area, including the zero-coverage spot users, and referring to the network in Figure 2, it can be noticed that the communication link between U_1 , U_3 , U_4 , and BS_1 is obstructed by obstacles.

At first, CSI_{ints} and CSI_{stat} are shared between the BS and HRIS controller, in which the CSI_{ints} contains the exact user location in regard to the continuous movement from the BS and HRIS. In the communication system network, the BS and HRIS are always fixed, resulting in the direct calculation of the user's exact location in reference to the HRIS at the HRIS controller (i.e., $D_{p(trans,ref)}$).

On the other hand, CSI_{stat} , known as the long-term CSI, will always share information with the HRIS controller about the possibility of the existence of an LoS with the HRIS in order to update the decision process.

Based on the information shared between the BS and the HRIS controller and the data on user location obtained from both, the signals received by the user can be written as in (9) and (10), in which they depend on the user being in the transmission or reflection area, respectively. The x_n represents the intended signal for the user n , where, for simplicity of clarification, $n = 1 : 4$, referring to the network in Figure 2.

$$x_t = 2PA_t \eta_{HRIS} e^{j\theta_t} x_n \quad (9)$$

$$x_r = 2PA_r \eta_{HRIS} e^{j\theta_r} x_n \quad (10)$$

Algorithm 1 Proposed HRIS decision-making function

Determine CSI_{inst} and CSI_{stat} for the network between BS_n and U
 $CSI_{inst} = vec(I_{response}, DF, d_{ue})$
 $CSI_{stat} = vec(FD, CH_{gain}, d_{ue}, LoS)$
if U in reflection area **then**
 while $D_{pref} = 1 \& D_{ptrans} = 0$ **do**
 calculate $P_{opposite}$
Ensure: $P = P_r$
 $x_r = P_r A_r \eta_{HRIS} e^{j\theta_r} x_n$
 end while
else U in transmission area
 while $D_{pref} = 0 \& D_{ptrans} = 1$ **do**
 calculate $P_{opposite}$
Ensure: $P = P_t$
 $x_t = P_t A_t \eta_{HRIS} e^{j\theta_t} x_n$
 end while
end if

The characteristics of the redirected signal for transmission and reflection are modelled in accordance with HRIS space wave impedance η_{HRIS} and the user location from the BS d_{ue} as in (11), where θ_i and $\theta_{r,t}$ are the incident and reflected or transmitted signal phase shifts, respectively, and η_0 is the space wave impedance constant.

$$\eta_{HRIS} = j \frac{\eta_0}{\cos \theta_i} \cot \left(\frac{(\sin \theta_i - \sin \theta_{r,t})}{2} \right) \cdot d_{ue} \quad (11)$$

As indicated in (9) and (10), the signal delivered to the user is associated with the power value P ; modelling this value is the most important part of the HRIS's functionality. As in the conventional T/R RIS, the power term is divided into two parts, one for transmission and the other for reflection, and as stated in (1), this means P can be rewritten as performed in (12).

To model the signal power in a hybrid manner, the location of the user in regard to the HRIS is addressed in the power calculation; thus, (12) is expressed as it is in (13), where the value of the factors $D_{p(trans,ref)}$, depending on the user location derived from the HRIS, will make the other signal power equal to zero. Substituting these values in (12) and (13) and extracting the power signal on the opposite side to $P_{opposite}$ equals $(SA_e A_t)$ in the case of reflection and $(SA_e A_r)$ in the case of transmission.

As a result of remodelling the signal power using the suggested power allocation, the power for transmission and reflection will follow (14), in which the full signal power will be allocated for either the transmitted or reflected signal simultaneously, keeping in mind the fact that the received signals, as in (9) and (10), will direct the signal for the intended user depending on θ_t and θ_r .

$$P = P_t + P_r \quad (12)$$

$$P = (S \times A_e \times D_{ptrans} \times A_t) + (S \times A_e \times D_{pref} \times A_r) \quad (13)$$

$$\begin{aligned} P_t &= (S \times A_e \times D_{ptrans} \times A_t) + P_{opposite} \\ \text{and} \\ P_r &= (S \times A_e \times D_{pref} \times A_r) + P_{opposite} \end{aligned} \quad (14)$$

where $S = \frac{|E_r|^2}{2Z_{air}}$, and $A_e = U_{AG} \frac{\lambda^2}{4\pi}$, in which the signal electric field E_r and the normalised radiation power NP are calculated in (15) and (16), respectively.

$$E_r = NPR_M \sqrt{2Z_{air} P_s U_{AG}^n A_{HRIS} G_{HRIS}} \quad (15)$$

$$NP = \frac{\sqrt{NP^{BS} NP^{HRIS,BS} NP^{HRIS,U} NP^U}}{4\pi l_{HRIS}^{BS} l_{HRIS}^U} \quad (16)$$

The proposed HRIS-DMA scheme introduces several innovations that contribute to efficient performance gains; the integration of DMA within the HRIS allows for precise and real-time control over signal reflection, significantly enhancing signal strength and coverage. The novel iterative algorithm continuously updates the HRIS configuration based on real-time user location data, optimising the signal path and reducing power loss and latency. The ability to adapt to changing network conditions and user locations ensures consistent and reliable performance, even in dynamic environments. Additionally, the proposed scheme minimises power consumption by focusing signal energy precisely where it is needed, thereby improving overall energy efficiency.

In order to determine the complexity equation for the HRIS-DMA method, we will analyse each individual component and then integrate them to create a comprehensive equation as follows:

1. Initialization Phase: complexity $O(1)$, this phase involves setting initial parameters, which is a constant time operation.
2. User Location Detection: complexity $O(n)$, this phase involves updating the locations of n users in real-time.
3. Signal Propagation and Reflection: complexity $O(M)$, this phase involves adjusting M elements in the HRIS to optimize signal reflection.
4. Real-Time Adjustment: complexity $O(n) \times O(M)$, this phase involves updating the HRIS configuration based on the real-time location data of n users and M HRIS elements.

Considering the most computationally intensive part of the algorithm (real-time adjustment), the overall complexity of the HRIS-DMA is dominated by the $O(n) \times O(M)$ term. Therefore, the complexity equation can be summarized as

$$O = O(1) + O(n) + O(M) + O(n) \times O(M) \quad (17)$$

Since $O(n) \times O(M)$ is the most significant term, the overall complexity simplifies to

$$O = O(n) \times O(M) \quad (18)$$

6. Implementation Scenarios

For ease of explanation, the downlink communication network in Figure 2 is explained first for the three performance evaluation scenarios: (1) zero to a few obstacles, (2) few to moderate obstacles, and (3) moderate to many obstacles. The communication network consists of four users referred to as U_1 , U_2 , U_3 , and U_4 ; one BS is referred to as BS_1 , and one HRIS located on top of a building is referred to as B_1 . As the network experiences different obstacle densities, users' locations are set in accordance to represent the three scenarios; U_3 is considered the first scenario, U_4 is considered the second scenario, and U_1 and U_2 are considered the third scenario. It is important to note that the actual performance test results used Table 3 parameters and were compared against the conventional T/R RIS and BS handover.

Table 3. Performance evaluation test parameters.

User Density (km ²)	THz Frequency
3×10^5	300 GHz
9×10^6	400 GHz
16×10^6	500 GHz

6.1. Zero to a Few Obstacles

In this scenario, there exists a LoS between BS₁ and U₃ but with few obstacles; in the case of fast movement or high winds, the network will suffer from high interference and the attenuation of the downlink signal. Although the BS's signals guarantee high signal quality and minimal latency, optimising the signal routes through the HRIS on top of B₁ will increase communication reliability with respect to higher interference and attenuation.

However, using the conventional T/R RIS will provide the user with the signal but at the cost of signal quality and latency since it can only serve one user at a time to transmit or reflect the signal. In the current example, there is only one user, but in the case of multiple users, this will result in a higher delay time.

On the other hand, using the current BS handover mechanism will generate 10% higher latency, keeping in mind that the signal will be received with better quality.

6.2. Few to Moderate Obstacles

The effect on downlink communication becomes more noticeable when moving to locations with more obstacles or obstacles of intermediate height. Barriers such as buildings or trees cause signal reflections, diffraction, and partial obstructions. In this scenario, U₄ is located in a zero-coverage spot, where there is NLoS with respect to BS₁. While adopting BS handover will provide the user with their intended signal, the transmission latency will be extremely high; this is because finding a different BS with a LoS with U₄ will cause extra overload in the network.

On the other hand, using the conventional T/R RIS will successfully deliver the signal for U₄, but there is a higher level of power loss with moderate coverage. This is because of the large distance between the user and the conventional T/R RIS. Alternatively, it could be because the user is in the transmission area, so the allocated signal power will be very low, making it impossible for the signal to reach the target U₄; as a result, this will affect the coverage area and reduce it.

During such situations, the HRIS adapts its surface configuration in real-time to minimise the impact of obstacles, optimising the transmission routes and compensating for any signal degradation. The new HRIS-DMA will enable the HRIS to transmit and reflect the incident signal simultaneously without any power loss.

Notably, the HRIS-DMA successfully remodels the signal power and phase and then redirects the signal to U₄ while the user is in the transmission area. It can be noticed here that the main focus is on the transmission area because the current state-of-the-art system splits the signal power in the conventional T/R RIS, which is the main drawback. The HRIS-DMA solves this drawback effectively and surpasses the conventional T/R RIS, especially for the application of the new wireless communication generation, 6G. Notwithstanding the difficulties, the system consistently sustains dependable downlink transmission, utilising the HRIS-DMA adaptability to improve the signal's strength and overcome insignificant obstacles.

6.3. Moderate to Many Obstacles

The last and most realistic wireless communication system scenario is an area with a high density of obstacles; downlink communication faces increased complexities in environments characterised by dense obstacles, such as urban areas with tall buildings or densely wooded regions featuring reflections, shadowing, and multipath fading impeding the signal propagation.

In accordance with the described area in Figure 2, U₁ and U₂ are located in highly obstacle-dense areas with NLoS between users and BS₁. In the downlink scenario, BS₁ fails to send the signals to their intended users; instead, BS₁ sends the signals to the HRIS element on top of B₁; the HRIS controller will analyse the incident signals using Algorithm 1 and redirect the signals toward U₁ and U₂ with full transmission power, resulting in a 100% coverage area.

The HRIS-DMA employs the novel iterative algorithm to actively and simultaneously

reconfigure the incident signal, creating focused signal paths and minimising the impact of obstacles on signal strength. Through adopting the HRIS-DMA, the downlink communication remains robust, ensuring effective data delivery to the user devices despite the challenges posed by the obstacle-dense environment.

As the stated examples mention only four users, the real-time test and performance analysis scenarios, which are shown in the following Section 7, prove the superiority of the proposed HRIS-DMA approach using the performance evaluation test parameters in Table 3, with higher and different density levels and a varied range of THz frequencies, making it a promising approach for deployment in 6G networks with THz applications.

7. Performance Analysis and Discussion

We initially analysed the performance of cooperative T/R RIS and BS-BS handover systems before investigating the performance of the HRIS-DMA and comparing the three. The performance analysis considers a highly dense user area, with 80% of the users having NLoS with respect to the BS. As the main purpose of this work is to provide a convenient solution for the power loss problem suffered by the conventional T/R RIS in the 6G era, we characterised the terahertz frequency band (300–500 GHz) for the evaluation process, as 6G is anticipated to work with this range of frequencies.

Firstly, we examined the amount of signal power loss with respect to the user density at 300 GHz operating frequency, as shown in Figure 4. It can be seen that as the number of users increases, the HRIS-DMA shows a stable performance with a maximum loss of 1.71 dBm, a conclusion that is in perfect agreement with the proposed algorithm. To be more precise, HRIS-DMA performs better than the T/R RIS as the tested area becomes denser; when the simulation reaches the maximum user density, the HRIS-DMA records 0.86 dBm signal power loss. On the contrary, using the T/R RIS shows 32 dBm power loss.

On the other hand, BS-BS handover performance regarding signal power loss showed relatively better results than the T/R RIS since the handover process did not split the signal power between two signals. However, the power loss can result from degradation, scattering, diffraction, and signal reflections. Table 4 summarises a comparison of power loss for different user density levels.

The HRIS-DMA method enables dynamic HRIS element adjustment to maximise signal reflection and propagation by including accurate user position data in the HRIS setup process. Comparing the HRIS-DMA methodology to the traditional way, Figure 4 shows how much less power loss there is. The suggested method minimises signal attenuation and maximises the effective power reaching the user, hence decreasing overall power loss, by dynamically modifying the HRIS elements to reflect signals effectively.

Table 4. Power loss comparison in (dBm).

Density	HRIS-DMA	T/R RIS	BS-BS
3×10^6	0.13	0.94	5.14
5×10^6	0.94	14.1	12.85
10×10^6	0.74	20.1	26
15×10^6	0.33	6.15	24.5

Figure 5 shows a comparison between the novel HRIS-DMA, T/R RIS, and BS-BS handover in terms of the latency that each system can produce for 300 GHz and the maximum user density of 16×10^6 ; the latency is observed for a maximum of 100 time signal transmissions. As noticed, the HRIS-DMA minimised the latency by 44% and 42% for BS-BS handover and T/R RIS, respectively.

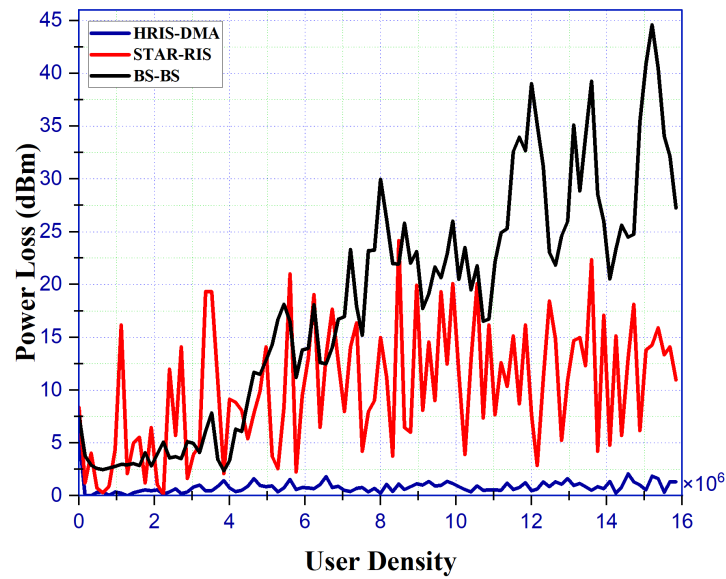


Figure 4. Power loss comparison.

In order to minimise reflection-induced delays and guarantee the most direct and efficient signal path, the iterative algorithm modifies the HRIS configuration continually. Figure 5 shows a significant decrease in latency for the HRIS-DMA method in comparison to the alternative. Through ensuring that the signal travels the quickest path to the user, the real-time flexibility and precise beamforming capabilities lower latency and speed up network response times.

To further highlight the enhancement of the HRIS-DMA in the network over T/R RIS and BS-BS handover, we compare the coverage area for the three approaches for 300, 400, and 500 GHz in Figure 6. It is evident from the results that the maximum coverage area that T/R RIS can provide is only 26% for users in the 300 GHz range; this is due to the fact that if the users are in a blocked area, and the distance between them and the T/R RIS is relatively long, the power associated with the signal will fade before reaching the intended user because T/R RISs transmit the signal with half of the power, as the T/R RIS divides the signal in order to transmit to the user located in the transmission area.

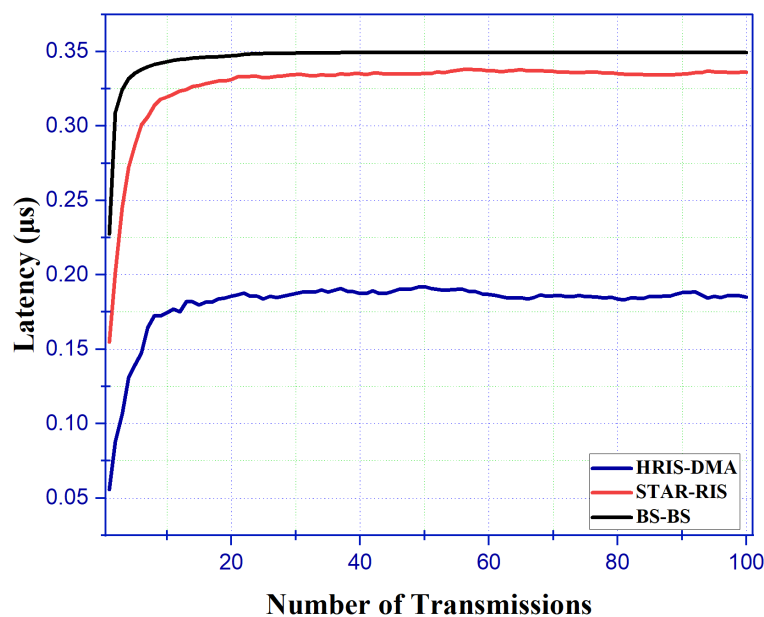


Figure 5. System delay for 300 GHz and 16×10^6 users.

By more successfully directing signals into under served locations, the HRIS-DMA technique expands the service area using intelligent reflection and beamforming. Comparing the HRIS-DMA methodology to the traditional method, Figure 6 shows a significant improvement in the coverage area. The suggested approach, which uses dynamic adjustment and real-time position data, can ensure better connectivity for users in larger and more complicated contexts by covering a greater area with a stronger signal.

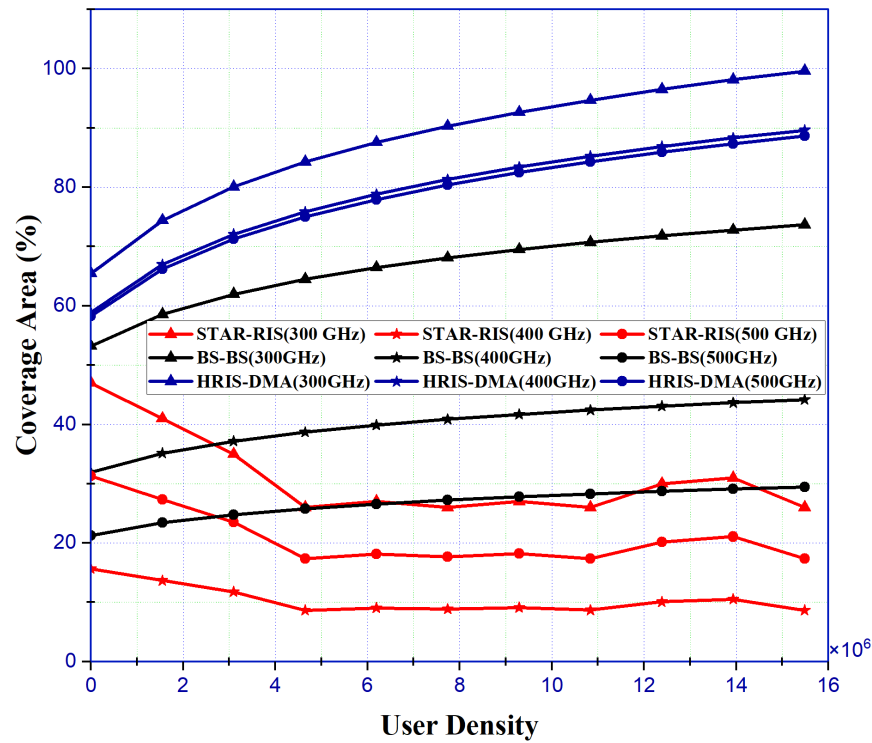


Figure 6. Comparative analysis of coverage area.

On the contrary, the HRIS-DMA successfully managed to provide 99.5% coverage under the same conditions. This superiority highlights the importance of the proposed decision-making algorithm, whether the user is located in the transmission or reflection area. Also, it can be noticed that the BS-BS handover performance is moderate between the HRIS-DMA and the T/R RIS, with exactly 74% coverage; this, on the other hand, proves that the HRIS-DMA successfully outperformed the current state-of-the-art transmission approaches. Table 5 summarises the simulation results for the different frequencies used.

Table 5. User coverage comparison.

Frequency (GHz)	HRIS-DMA	T/R RIS	BS-BS
300	99.5%	26%	74%
400	90%	9%	44%
500	88.5%	17%	29%

Furthermore, as the communication system being tested operates in places with a significant number of users and obstacles, we identified and calculated the failed signal rate (FSR), which computes the total number of undelivered signals to users in regard to the total number of signals that were meant to be delivered to users. The results of this metric indicate that the HRIS-DMA outperformed the other approaches, as shown in Figures 7 and 8, for different user densities and THz frequencies.

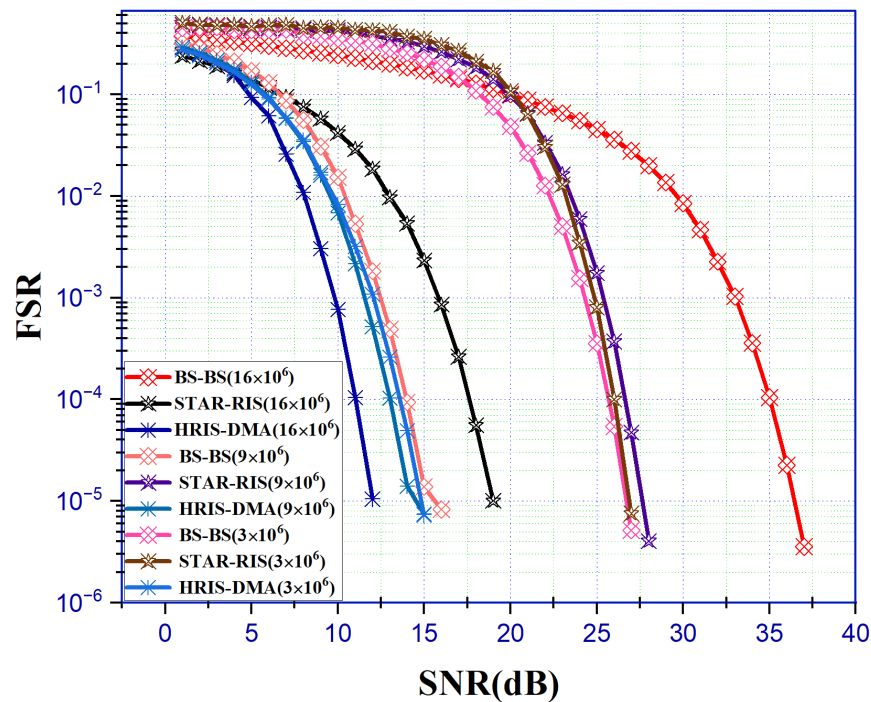


Figure 7. FSR comparison for different user densities and 300 GHz.

First, we measured the FSR for different user densities in order to gain a clear idea of the HRIS-DMA performance stability. As shown in Figure 7, using the HRIS-DMA in the network with a user density of 3×10^6 under a 300 GHz operating frequency yields a 12 dB channel gain compared to the T/R RIS and BS-BS handover, where the performance of the T/R RIS relatively matches the performance of BS handover at the lowest density tested. In regard to a higher density level of 9×10^6 users, the HRIS-DMA and BS-BS handover approximately show the same performance, with only 1 dB channel gain achieved by the HRIS-DMA; oppositely, the channel gain achieved by the HRIS-DMA reached 13 dB compared to that for T/R RIS.

As the HRIS-DMA performance should satisfy the requirement of 6G wireless generation, a higher density level must be considered, with a 16×10^6 user. Evidently, from Figure 7, as the density increased, the performance of both the T/R RIS and BS-BS handover dropped; in this regard, the achieved channel gain for HRIS-DMA reaches 25 dB with regard to the T/R RIS. These promising results motivate the analysis of the HRIS-DMA performance for 400 and 500 GHz, which is shown in Figure 8.

Iterative updates to the HRIS configuration, which are influenced by the user's location, contribute to the maintenance of robust and consistent signal connections. The HRIS-DMA methodology has a decreased FSR compared to the conventional method, as Figures 7 and 8 demonstrate. The signal path is controlled dynamically and precisely to maintain consistent signal quality and robustness, even in difficult conditions, thus minimising the chances of signal failures.

It is evident from Figure 8 that the HRIS-DMA has an excellent stable performance compared to the T/R RIS and BS-BS handover, achieving 26 dB and 8 dB channel gain, respectively. Achieving stable ideal performance in wireless communication is crucial to ensuring a consistent and satisfactory user experience.

Finally, to confirm the consistent and dependable performance of the HRIS-DMA, taking into account the aforementioned validation metrics, we conducted 100 repeated tests with identical operating settings and features to assess the accuracy of the results. As depicted in Figure 9, the HRIS-DMA exhibits system dependability and stability of 95%, whereas the T/R RIS only maintained a system reliability of 11% during these tests. Implementing the HRIS-DMA in the wireless communication system led to a significant

increase in reliability of 81%.

The HRIS-DMA technique improves system efficiency by optimising energy utilisation and minimising signal loss to ensure optimal user reception. Figure 9 demonstrates that the HRIS-DMA strategy achieves greater system efficiency than the conventional way. The suggested method optimises network efficiency by reducing power loss and enhancing signal strength and coverage. This results in improved performance and decreased energy consumption.

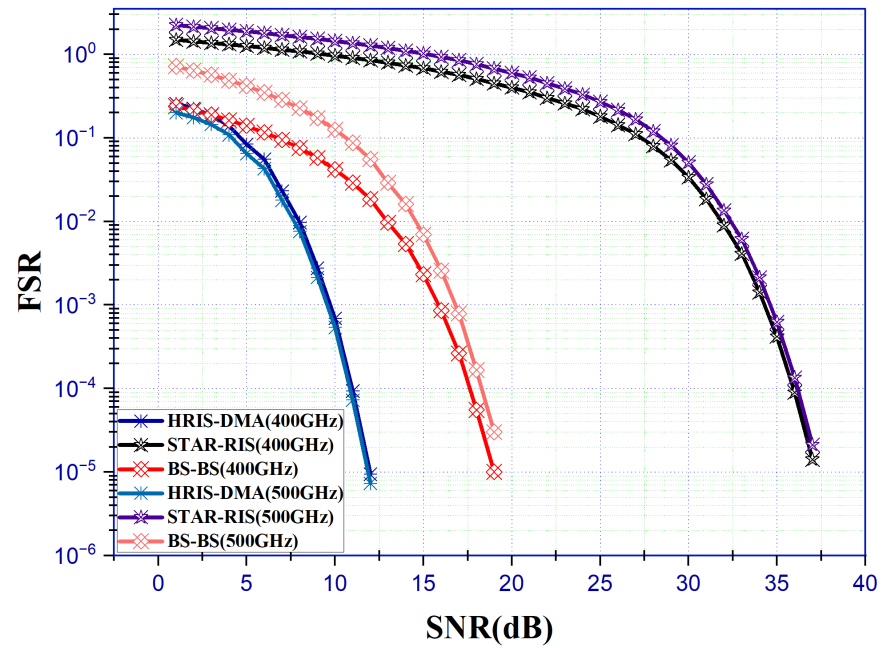


Figure 8. FSR comparison for different THz frequencies and 16×10^6 users.

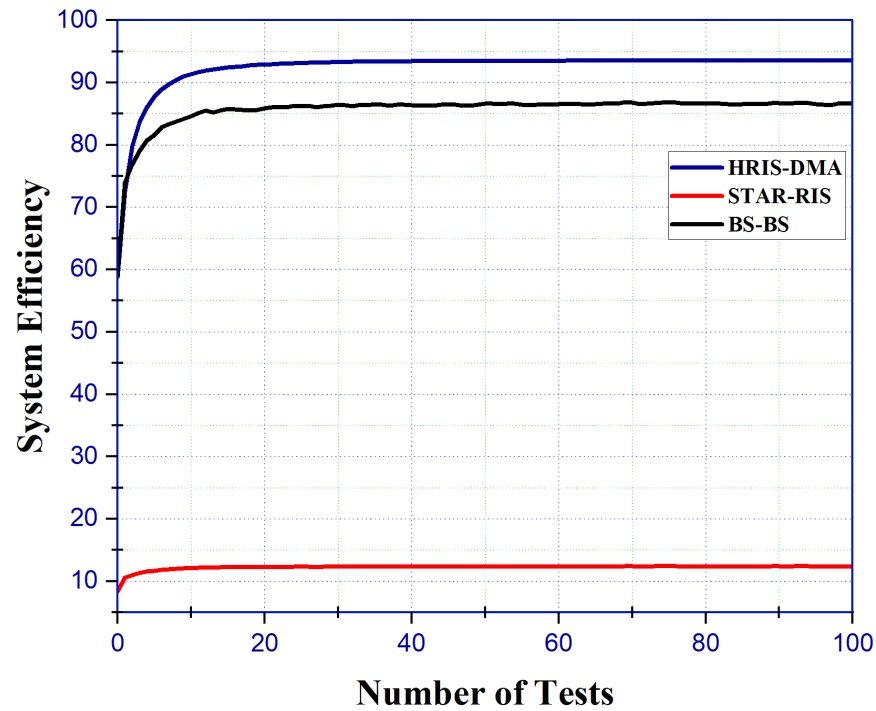


Figure 9. Overall system efficiency.

8. Conclusions

In this work, we provide a novel idea of a hybrid reconfigurable intelligent surface decision-making algorithm to eliminate the signal power loss and limited coverage area of the conventional T/R RIS and the high delay of BS-BS handover. HRIS-DMA uses the exact user location to provide the user with maximum power coverage. The numerical results confirm the superiority of the proposed HRIS-DMA algorithm over existing conventional approaches. Using the HRIS-DMA saves up to 70% of signal power, potentially providing 100% coverage and 45% less delay. These results provide the potential and effective use of HRIS-DMA for the new wireless generation of 6G and its diverse range of applications.

In this work, we managed to achieve reduced power loss, which is achieved through dynamic adjustment and optimal signal reflection; lower latency, due to real-time adaptability and efficient signal paths; enhanced coverage area, through intelligent beamforming and reflection; a lower failed signal rate, ensured by strong and stable signal connections; and improved system efficiency, resulting from optimised energy utilisation and reduced power loss.

The application of the proposed HRIS-DMA approach in 6G networks offers several advantages. In urban environments with high building density, RISs can be strategically placed on building facades to direct signals around obstacles, ensuring continuous and reliable connectivity. In indoor settings such as large commercial complexes, RISs can enhance coverage by reflecting signals into areas that are typically hard to reach, such as basements or isolated rooms. Additionally, in vehicular networks, RISs can dynamically adjust to the movement of vehicles, providing stable and high-quality communication links. By leveraging the exact user location data, our approach ensures that the benefits of RIS technology are fully realised, leading to improved network performance and user experience in various 6G deployment scenarios.

Author Contributions: Conceptualisation; methodology; software; validation; formal analysis; investigation; resources; data curation; writing—original draft preparation; writing—review and editing; and visualisation, A.K.A.; supervision and review, H.S.A.-R. All authors have read and agreed to the published version of the manuscript.

Funding: This research received no external funding.

Data Availability Statement: Derived data supporting the findings of this study are available from the corresponding author upon request.

Conflicts of Interest: The authors declare no conflicts of interest.

Abbreviations

The following abbreviations are used in this manuscript:

5G	Fifth Generation;
6G	Sixth Generation;
AI	Artificial Intelligence;
AP	Access Point;
BS	Base Station;
EE	Energy Efficiency;
ES	Energy Splitting;
FSR	Failed Signal Rate
HRIS-DMA	Hybrid Reconfigurable Intelligent Surface— Decision-Making Algorithm;
IOS	Intelligent Omni Surface;
IoT	Internet of Things;
LoS	Line of Sight;
MIMO	Multiple-Input Multiple-Output;
MISO	Multiple-Input Single-Output;
MS	Mode Switching;
NLoS	No Line of Sight;
PIN	Positive-Intrinsic-Negative;

RF	Radio Frequency;
RIS	Reconfigurable Intelligent Surface;
SNR	Signal-to-Noise Ratio;
SU-MIMO	Single-User Multiple-Input Multiple-Output;
THz	Terahertz;
TS	Time Switching;
T/R RIS	Transmissive Reflective Reconfigurable Intelligent Surface;
UAV	Unmanned Aerial Vehicle;
UDNs	Ultra-Dense Networks;
UE	User Equipment;
UM-MIMO	Ultra-Massive Multiple-Input Multiple-Output.

References

- Wang, C.X.; You, X.; Gao, X.; Zhu, X.; Li, Z.; Zhang, C.; Wang, H.; Huang, Y.; Chen, Y.; Haas, H.; et al. On the Road to 6G: Visions, Requirements, Key Technologies, and Testbeds. *IEEE Commun. Surv. Tutorials* **2023**, *25*, 905–974. [[CrossRef](#)]
- Corici, M.I.; Eichhorn, F.; Bless, R.; Gundall, M.; Lindenschmitt, D.; Bloessl, B.; Petrova, M.; Wimmer, L.; Kreuch, R.; Magedanz, T.; et al. Organic 6G Networks: Vision, Requirements, and Research Approaches. *IEEE Access* **2023**, *11*, 70698–70715. [[CrossRef](#)]
- Imam-Fulani, Y.O.; Faruk, N.; Sowande, O.A.; Abdulkarim, A.; Alozie, E.; Usman, A.D.; Adewole, K.S.; Oloyede, A.A.; Chiroma, H.; Garba, S.; et al. 5G Frequency Standardization, Technologies, Channel Models, and Network Deployment: Advances, Challenges, and Future Directions. *Sustainability* **2023**, *15*, 5173. [[CrossRef](#)]
- Hassouna, S.; Jamshed, M.A.; Rains, J.; Kazim, J.u.R.; Rehman, M.U.; Abualhayja, M.; Mohjazi, L.; Cui, T.J.; Imran, M.A.; Abbasi, Q.H. A survey on reconfigurable intelligent surfaces: Wireless communication perspective. *IET Commun.* **2023**, *17*, 497–537. [[CrossRef](#)]
- Alves Junior, M.A.; Fraidenraich, G.; Ferreira, R.C.; De Figueiredo, F.A.P.; De Lima, E.R. Multiple-Antenna Weibull-Fading Wireless Communications Enhanced by Reconfigurable Intelligent Surfaces. *IEEE Access* **2023**, *11*, 107218–107236. [[CrossRef](#)]
- Liu, R.; Li, M.; Luo, H.; Liu, Q.; Swindlehurst, A.L. Integrated Sensing and Communication with Reconfigurable Intelligent Surfaces: Opportunities, Applications, and Future Directions. *IEEE Wirel. Commun.* **2023**, *30*, 50–57. [[CrossRef](#)]
- Qu, K.; Chen, K.; Zhao, J.; Zhang, N.; Hu, Q.; Zhao, J.; Jiang, T.; Feng, Y. An electromechanically reconfigurable intelligent surface for enhancing sub-6G wireless communication signal. *J. Intf. Intell.* **2023**, *1*, 207–216. [[CrossRef](#)]
- Lu, H.; Zeng, Y.; Jin, S.; Zhang, R. Aerial Intelligent Reflecting Surface: Joint Placement and Passive Beamforming Design With 3D Beam Flattening. *IEEE Trans. Wirel. Commun.* **2021**, *20*, 4128–4143. [[CrossRef](#)]
- Ye, J.; Guo, S.; Dang, S.; Shihada, B.; Alouini, M.S. On the Capacity of Reconfigurable Intelligent Surface Assisted MIMO Symbiotic Communications. *IEEE Trans. Wirel. Commun.* **2022**, *21*, 1943–1959. [[CrossRef](#)]
- Xing, Z.; Wang, R.; Yuan, X. Joint Active and Passive Beamforming Design for Reconfigurable Intelligent Surface Enabled Integrated Sensing and Communication. *IEEE Trans. Commun.* **2023**, *71*, 2457–2474. [[CrossRef](#)]
- Yin, T.; Li, L.; Lin, W.; Hu, H.; Ma, D.; Liang, J.; Bai, T.; Pan, C.; Han, Z. Joint Active and Passive Beamforming Optimization for Multi-IRS-Assisted Wireless Communication Systems: A Covariance Matrix Adaptation Evolution Strategy. *IEEE Trans. Veh. Technol.* **2023**, *72*, 9281–9292. [[CrossRef](#)]
- Chu, Z.; Xiao, P.; Mi, D.; Yin, C.; Hao, W.; Liu, W.; Sodre, A.C. Jointly Active and Passive Beamforming Designs for IRS-Empowered WPCN. *IEEE Internet Things J.* **2023**, *11*, 11579–11592. [[CrossRef](#)]
- Elsherbini, M.M.; Omer, O.A.; Salah, M. Reconfigurable Intelligent Surface Reliable Cooperative Beamforming Based on Cascade/Parallel Hybrid Networking. *IEEE Access* **2023**, *11*, 65255–65265. [[CrossRef](#)]
- Zhang, S.; Yang, Z.; Chen, M.; Liu, D.; Wong, K.K.; Vincent Poor, H. Beamforming Design for the Performance Optimization of Intelligent Reflecting Surface Assisted Multicast MIMO Networks. *IEEE Trans. Wirel. Commun.* **2023**, *23*, 2325–2339. [[CrossRef](#)]
- Aung, P.S.; Park, Y.M.; Tun, Y.K.; Han, Z.; Hong, C.S. Energy-Efficient Communication Networks via Multiple Aerial Reconfigurable Intelligent Surfaces: DRL and Optimization Approach. *IEEE Trans. Veh. Technol.* **2023**, *73*, 4277–4292. [[CrossRef](#)]
- Singh, J.; Srivastava, S.; Yadav, S.P.; Jagannatham, A.K.; Hanzo, L. Energy Efficiency Optimization in Reconfigurable Intelligent Surface Aided Hybrid Multiuser mmWave MIMO Systems. *IEEE Open J. Veh. Technol.* **2023**, *4*, 581–589. [[CrossRef](#)]
- Wang, Y.; Peng, J. Energy Efficiency Fairness of Active Reconfigurable Intelligent Surfaces-Aided Cell-Free Network. *IEEE Access* **2023**, *11*, 5884–5893. [[CrossRef](#)]
- Goh, C.Y.; Leow, C.Y.; Nordin, R. Energy Efficiency of Unmanned Aerial Vehicle with Reconfigurable Intelligent Surfaces: A Comparative Study. *Drones* **2023**, *7*, 98. [[CrossRef](#)]
- Zhang, C.; Lu, H.; Chen, C.W. Reconfigurable Intelligent Surfaces-Enhanced Uplink User-Centric Networks on Energy Efficiency Optimization. *IEEE Trans. Wirel. Commun.* **2023**, *22*, 9013–9028. [[CrossRef](#)]
- Ge, Y.; Fan, J.; Zhang, J. Active Reconfigurable Intelligent Surface Enhanced Secure and Energy-Efficient Communication of Jittering UAV. *IEEE Internet Things J.* **2023**, *10*, 22386–22400. [[CrossRef](#)]
- Tan, F.; Xu, X.; Chen, H.; Li, S. Energy-efficient beamforming optimization for MISO communication based on reconfigurable intelligent surface. *Phys. Commun.* **2023**, *57*, 101996. [[CrossRef](#)]

22. Sun, S.; An, N.; Yang, F.; Song, J.; Han, Z. Capacity Characterization Analysis of Optical Intelligent Reflecting Surface Assisted MISO VLC. *IEEE Internet Things J.* **2023**, *11*, 4801–4814. [[CrossRef](#)]
23. Chen, J.; Liang, Y.C.; Cheng, H.V.; Yu, W. Channel Estimation for Reconfigurable Intelligent Surface Aided Multi-User mmWave MIMO Systems. *IEEE Trans. Wirel. Commun.* **2023**, *22*, 6853–6869. [[CrossRef](#)]
24. Mekonnen, F.D.; Tulu, M.M.; Meko, S.F. Performance Analysis of Large Intelligent Reflecting Surface Aided Moderate MIMO for 5G Communication. *Wirel. Pers. Commun.* **2023-07-01**, *131*, 1033–1049. [[CrossRef](#)]
25. Sun, S.; Yang, F.; Song, J.; Zhang, R. Intelligent Reflecting Surface for MIMO VLC: Joint Design of Surface Configuration and Transceiver Signal Processing. *IEEE Trans. Wirel. Commun.* **2023**, *22*, 5785–5799. [[CrossRef](#)]
26. Weiqiang Tan, Q.Z.; Weijie Tan, L.Y.; Li, C. Performance Analysis of Intelligent Reflecting Surface Assisted Wireless Communication System. *Comput. Model. Eng. Sci.* **2023**, *137*, 775–787. [[CrossRef](#)]
27. Zhang, Y.; You, C.; Zheng, B. Multi-Active Multi-Passive (MAMP)-IRS Aided Wireless Communication: A Multi-Hop Beam Routing Design. *IEEE J. Sel. Areas Commun.* **2023**, *41*, 2497–2513. [[CrossRef](#)]
28. Wei, T.; Wu, L.; Mishra, K.V.; Shankar, M.R.B. Multi-IRS-Aided Doppler-Tolerant Wideband DFRC System. *IEEE Trans. Commun.* **2023**, *71*, 6561–6577. [[CrossRef](#)]
29. Das, P.; Basak, S.; Vishwakarma, P.; Singh, A.K.; Sur, S.N. Performance analysis of IRS-aided multi-user millimeter wave communications system. *Int. J. Inf. Technol.* **2023**, *16*, 799–808. [[CrossRef](#)]
30. Liang, R.; Fan, J. Energy-Efficient mmWave IoT Communications With Multihop IRS-Assisted Systems. *IEEE Internet Things J.* **2023**, *10*, 19344–19355. [[CrossRef](#)]
31. Wang, H.; Shi, Z.; Fu, Y.; Song, R. Downlink Multi-IRS Aided NOMA System With Second-Order Reflection. *IEEE Wirel. Commun. Lett.* **2023**, *12*, 1022–1026. [[CrossRef](#)]
32. Amiriara, H.; Ashtiani, F.; Mirmohseni, M.; Nasiri-Kenari, M. IRS-User Association in IRS-Aided MISO Wireless Networks: Convex Optimization and Machine Learning Approaches. *IEEE Trans. Veh. Technol.* **2023**, *72*, 14305–14316. [[CrossRef](#)]
33. Song, Y.; Xu, S.; Sun, G.; Ai, B. Weighted Sum-Rate Maximization in Multi-IRS-Aided Multi-Cell mmWave Communication Systems for Suppressing ICI. *IEEE Trans. Veh. Technol.* **2023**, *72*, 10234–10250. [[CrossRef](#)]
34. Wang, J.; Ni, H. Path loss modeling and performance evaluation of double IRSs-aided wireless communication systems based on spatial scattering channel model. *Sci. Rep.* **2023**, *13*, 8400. [[CrossRef](#)] [[PubMed](#)]
35. Liu, Y.; Mu, X.; Xu, J.; Schober, R.; Hao, Y.; Poor, H.V.; Hanzo, L. STAR: Simultaneous Transmission and Reflection for 360° Coverage by Intelligent Surfaces. *IEEE Wirel. Commun.* **2021**, *28*, 102–109. [[CrossRef](#)]
36. Xu, J.; Liu, Y.; Mu, X.; Dobre, O.A. STAR-RISs: Simultaneous Transmitting and Reflecting Reconfigurable Intelligent Surfaces. *IEEE Commun. Lett.* **2021**, *25*, 3134–3138. [[CrossRef](#)]
37. Mu, X.; Liu, Y.; Guo, L.; Lin, J.; Schober, R. Simultaneously Transmitting and Reflecting (STAR) RIS Aided Wireless Communications. *IEEE Trans. Wirel. Commun.* **2022**, *21*, 3083–3098. [[CrossRef](#)]
38. Zhang, S.; Zhang, H.; Di, B.; Tan, Y.; Di Renzo, M.; Han, Z.; Vincent Poor, H.; Song, L. Intelligent Omni-Surfaces: Ubiquitous Wireless Transmission by Reflective-Refractive Metasurfaces. *IEEE Trans. Wirel. Commun.* **2022**, *21*, 219–233. [[CrossRef](#)]
39. Feng, Y.; Zhu, B.; Chen, K.; Zhao, J.; Jiang, T. Dynamically controlling electromagnetic wave with tunable metasurfaces. In Proceedings of the 2015 International Symposium on Antennas and Propagation (ISAP), Hobart, Australia, 9–12 November 2015; pp. 1–4.
40. Zhang, S.; Zhang, H.; Di, B.; Tan, Y.; Han, Z.; Song, L. Beyond Intelligent Reflecting Surfaces: Reflective-Transmissive Metasurface Aided Communications for Full-Dimensional Coverage Extension. *IEEE Trans. Veh. Technol.* **2020**, *69*, 13905–13909. [[CrossRef](#)]
41. Alexandropoulos, G.C.; Shlezinger, N.; Alamzadeh, I.; Imani, M.F.; Zhang, H.; Eldar, Y.C. Hybrid Reconfigurable Intelligent Metasurfaces: Enabling Simultaneous Tunable Reflections and Sensing for 6G Wireless Communications. *IEEE Veh. Technol. Mag.* **2023**, *19*, 75–84. [[CrossRef](#)]
42. Wang, W.; Song, K. Hybrid Active–Passive Reconfigurable Intelligent Surface for Cooperative Transmission Systems. *Appl. Sci.* **2024**, *14*, 231. [[CrossRef](#)]
43. Soleymani, M.; Santamaria, I.; Jorswieck, E.A. Spectral and Energy Efficiency Maximization of MISO STAR-RIS-Assisted URLLC Systems. *IEEE Access* **2023**, *11*, 70833–70852. [[CrossRef](#)]
44. Li, M.; Zhang, S.; Ge, Y.; Li, Z.; Gao, F.; Fan, P. STAR-RIS Aided Integrated Sensing and Communication over High Mobility Scenario. *IEEE Trans. Commun.* **2024**, *1*, Early Access. [[CrossRef](#)]
45. Papazafeiropoulos, A.; Kourtessis, P.; Chatzinotas, S. STAR-RIS-Assisted Communication Radar Coexistence: Analysis and Optimization. *IEEE Trans. Veh. Technol.* **2024**, 1–14. Early Access. [[CrossRef](#)]
46. Aung, P.S.; Nguyen, L.X.; Tun, Y.K.; Han, Z.; Hong, C.S. Aerial STAR-RIS Empowered MEC: A DRL Approach for Energy Minimization. *IEEE Wirel. Commun. Lett.* **2024**, *13*, 1409–1413. [[CrossRef](#)]
47. Wei, W.; Pang, X.; Xing, C.; Zhao, N.; Niyato, D. STAR-RIS Aided Secure NOMA Integrated Sensing and Communication. *IEEE Trans. Wirel. Commun.* **2024**, *1*, Early Access. [[CrossRef](#)]
48. Wen, Y.; Chen, G.; Fang, S.; Chu, Z.; Xiao, P.; Tafazolli, R. STAR-RIS-Assisted-Full-Duplex Jamming Design for Secure Wireless Communications System. *IEEE Trans. Inf. Forensics Secur.* **2024**, *19*, 4331–4343. [[CrossRef](#)]
49. Li, N.; Chen, B.; Tao, X. STAR-RIS Assisted Offloading Based on Hybrid NOMA: A Time Minimization Perspective. *IEEE Trans. Veh. Technol.* **2024**, 1–16. Early Access. [[CrossRef](#)]

50. Yang, S.; Ding, Z.; Zhu, H. STAR-RIS Aided Multi-Antenna NOMA Downlink and Uplink Transmissions: A Low-Complexity Approach. *IEEE Trans. Wirel. Commun.* **2024**, *1*, Early Access. [[CrossRef](#)]
51. Papazafeiropoulos, A.; Ge, H.; Kourtessis, P.; Ratnarajah, T.; Chatzinotas, S.; Papavassiliou, S. Two-Timescale Design for Active STAR-RIS Aided Massive MIMO Systems. *IEEE Trans. Veh. Technol.* **2024**, *73*, 10118–10134. [[CrossRef](#)]
52. Gunasinghe, D.; Kudathanthirige, D.; Baduge, G.A.A. The Achievable Rate Performance of STAR-RIS Aided Massive MIMO Systems. *IEEE Trans. Commun.* **2024**, *72*, 3681–3700. [[CrossRef](#)]
53. Katwe, M.; Deshpande, R.; Singh, K.; Pan, C.; Ghare, P.H.; Duong, T.Q. Spectrally-Efficient Beamforming Design for STAR-RIS-aided URLLC NOMA Systems. *IEEE Trans. Commun.* **2024**, *72*, 4414–4431. [[CrossRef](#)]
54. Zhang, Y.; Yang, L.; Li, X.; Guo, K.; Liu, H. Covert Communications for STAR-RIS-Assisted Industrial Networks With a Full Duplex Receiver and RSMA. *IEEE Internet Things J.* **2024**, *11*, 22483–22493. [[CrossRef](#)]
55. Farhadi, A.; Moomivand, M.; Taskou, S.K.; Mili, M.R.; Rasti, M.; Hossain, E. A Meta-DDPG Algorithm for Energy and Spectral Efficiency Optimization in STAR-RIS-Aided SWIPT. *IEEE Wirel. Commun. Lett.* **2024**, *13*, 1473–1477. [[CrossRef](#)]
56. Wu, Q.; Zhang, R. Towards Smart and Reconfigurable Environment: Intelligent Reflecting Surface Aided Wireless Network. *IEEE Commun. Mag.* **2020**, *58*, 106–112. [[CrossRef](#)]
57. Ihsan, A.; Chen, W.; Asif, M.; Khan, W.U.; Wu, Q.; Li, J. Energy-Efficient IRS-Aided NOMA Beamforming for 6G Wireless Communications. *IEEE Trans. Green Commun. Netw.* **2022**, *6*, 1945–1956. [[CrossRef](#)]
58. Huang, C.; Zappone, A.; Alexandropoulos, G.C.; Debbah, M.; Yuen, C. Reconfigurable Intelligent Surfaces for Energy Efficiency in Wireless Communication. *IEEE Trans. Wirel. Commun.* **2019**, *18*, 4157–4170. [[CrossRef](#)]

Disclaimer/Publisher’s Note: The statements, opinions and data contained in all publications are solely those of the individual author(s) and contributor(s) and not of MDPI and/or the editor(s). MDPI and/or the editor(s) disclaim responsibility for any injury to people or property resulting from any ideas, methods, instructions or products referred to in the content.